19th Australasian Fluid Mechanics Conference
Melbourne, Australia
8-11 December 2014

Reynolds Number Effects on the Aerodynamic Performance of Wing Planform Shapes in Hover

A. Shahzad, F.B. Tian, J. Young, and J.C.S. Lai

School of Engineering and Information Technology
The University of New South Wales, Canberra, ACT 2601, Australia

Abstract

The parameters of wing geometry such as wing planform shape influence the aerodynamic performance of insects, birds and micro aerial vehicles (MAV). Past research has shown contrasting results about the effect of wing planform shapes on the aerodynamic performance of a wing in hover. This study is focused on comparing the performance of four wing shapes (three wings with different wing area distribution defined by the radius of the first moment of wing area ($\bar{r}_1$), and a rectangular wing) at Reynolds number (Re) = 12, 400 and 13500 with hovering kinematics. An immersed boundary method was employed to solve the 3D, viscous, incompressible Navier–Stokes equations. The average lift coefficient and peak lift coefficient were found to increase with both increasing outboard wing area, and increasing Re. Wings with less wing area distribution outboard were more efficient at all Re, provided they generated enough lift to maintain hovering flight. The similarity in time history of lift coefficient, average lift coefficient and power economy of the rectangular and $\bar{r}_1$ = 0.53 wings at Re = 12 suggest that $\bar{r}_1$ may be important in determining the performance of wings especially at low Re.

Introduction

The geometric parameters and kinematics of insect wings and their effects on the aerodynamic performance in hovering flight have attracted great attention in the past. However, previous studies on aerodynamic performance of wing planform shapes have shown contrasting results. In a computational study at Re = 200 and 3500, Luo and Sun [5] reported a difference of less than 5% in the force coefficients for ten different wing shapes (with fruit fly wing as a reference) rotating at constant angle of attack. In an experimental study, Ozen and Rockwell [6] reported qualitatively similar flow structures for rectangle and fruit fly wings. While Phillips et al. [7] also reported similarity in flow structures for rectangle, ellipse, four ellipse and reverse ellipse wings, the findings of the study of Ansari et al. [1] and the computational studies of Wilkins [10] and Tejas [2] are different. Ansari et al. [1] and Wilkins [10] found that keeping more wing area outboard generally increases the force coefficients but it could result in reduced efficiency because of increasing power requirements. Tejas [2] compared the performance of a rectangular wing, ellipse, reverse ellipse, four ellipse and a triangular wing at Re = 12, 1134 and 13500 using a Navier–Stokes (N-S) solver with thrips, honeybee and two angle kinematics respectively. It was found that the results at Re = 1134 and 13500 are similar to those of Ansari et al. [1] and Wilkins [10]. However, at Re = 12, the wing with a larger area outboard (reverse ellipse), did not produce the highest values of force coefficients, but it outperformed others in performance efficiency. It is interesting to note that according to Tejas [2], the best performance efficiency at Re = 12, 1134 and 13500 is achieved by the reverse ellipse, ellipse and rectangular wing shape respectively. Hence, the effects of Reynolds numbers on the aerodynamic performance of wing shapes (with a variety of wing area distribution) need to be investigated further.

The aim of this study is to investigate the aerodynamic performance of wing shapes with different wing area distributions at three Re values: 12, 400 and 13500, to represent flow regimes with qualitatively different leading edge vortex structures, and viscous and inertial effects. The Reynolds numbers are approximately those of thrips, hoverflies and MAVs. The results obtained may be used to interpret the aerodynamic performance of wing shapes of insects with various sizes operating at different Reynolds numbers.

Wing Geometry and Kinematics

The wing shapes of insects can be reasonably approximated by the beta distribution [3], which can generate shapes with straight leading edge, constant wing length and area. This is achieved by changing only one parameter, $\bar{r}_1$. Following equations are taken from Ellington [3] for the generation of wing shapes:

$$\bar{r}_1 = \int_0^1 \bar{c}.\bar{r}\, d\bar{r} \quad (1)$$

$$\bar{r}_2 = 0.929(\bar{r}_1)^{0.732} \quad (2)$$

$$p = \bar{r}_1\left(\frac{\bar{r}_1(1-\bar{r}_1)}{\bar{r}_2^2-\bar{r}_1^2} - 1\right) \quad (3)$$

$$q = (1-\bar{r}_1)\left(\frac{\bar{r}_1(1-\bar{r}_1)}{\bar{r}_2^2-\bar{r}_1^2} - 1\right) \quad (4)$$

$$B(p,q) = \int_0^1 \bar{r}^{p-1}(1-\bar{r})^{q-1} d\bar{r} \quad (5)$$

$$\bar{c} = \frac{\bar{r}^{p-1}(1-\bar{r})^{q-1}}{B(p,q)} \quad (6)$$

Here $\bar{c}$ is chord length normalized by mean chord, $\bar{r}$ is distance from the wing base normalized by wing length, $\bar{r}_1$ and $\bar{r}_2$ are respectively non-dimensional radius of the first moment and second moment of the wing area, and $B(p,q)$ is the beta function defined by two parameters p and q. These parameters are calculated by radii of first two moments of wing area. The wing shapes presented in figure 1, normalized by mean chord (c) include three beta distribution wings: $\bar{r}_1$ = 0.43, 0.53 and 0.63, and a rectangular wing.

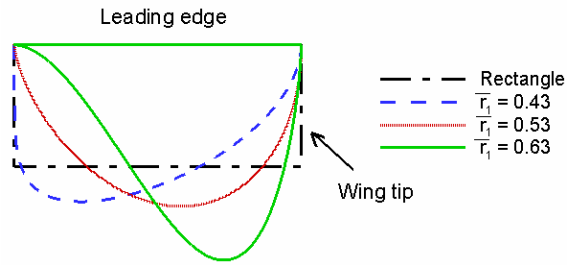

Figure 1. Wing shapes. Mean chord = 27.7mm, wing length = 82 mm.

The kinematics of Phillips [7] shown in figure 2 have been used in the study. The wing flaps in a horizontal stroke plane with no elevation angle. The pitch axis is located at 0.25*c* from the leading edge. Roots of the wing shapes under consideration are different. Hence, the pivot is not kept at the root and it is offset by a constant value (0.87c) from the wing root for all the wings to ensure fair comparison.

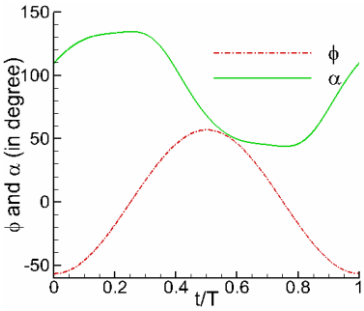

Figure 2. Wing kinematics. Flap angle, Φ and pitch angle α.

Computational Method

The numerical simulations are carried out with a viscous, 3D, incompressible N–S solver [8] based on a second order sharp interface immersed boundary method. The wing surface is meshed with unstructured triangular elements, and the flow is computed on a non-uniform Cartesian grid in the domain as presented in figure 3. The flow is assumed to be laminar. No slip and no penetration boundary conditions are imposed on the wing, and the domain is extended by 20*c* in all directions.

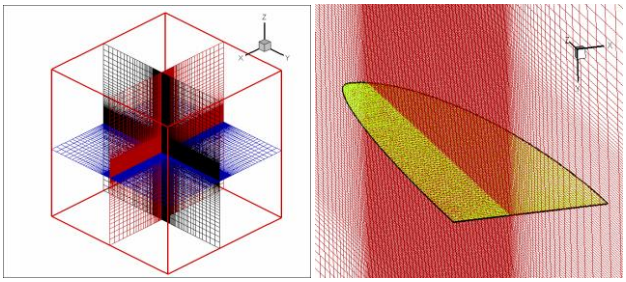

Figure 3. Cartesian grid in background and close up of mesh on a Zimmerman wing planform used in the validation study.

Validation

Grid independence and time independence studies are conducted using a $\bar{r_1}$ = 0.63 wing at Re = 13500. For grid independence, simulations are performed on background meshes of approximately 5 million (coarse), 10 million (medium) and 20 million cells (fine) with 4000 time steps per flapping cycle. For time independence, the medium grid is run with 2000, 4000 and 6000 time steps per flapping cycle. Details of the validation studies are presented in table 1.

Grid	Time steps	i × j × k	$\overline{C_L}$	$\overline{C_P}$
1. Grid independence				
Coarse	4000	179 × 127 × 221	0.950	1.252
Medium		233 × 155 × 295	0.996	1.317
Fine		287 × 183 × 369	1.014	1.345
2. Time independence				
Medium	2000	233 × 155 × 295	1.028	1.365
	4000		0.999	1.313
	6000		0.974	1.286

Table 1. Results of grid independence and time independence

The difference of average lift coefficient ($\overline{C_L}$) and average power coefficient ($\overline{C_P}$) between the medium and fine grid is 1.8% and 2.1% respectively. The difference of $\overline{C_L}$ and $\overline{C_P}$ between the medium and fine time steps is 2.6% and 2.1% respectively. Based on these results, the medium mesh with 4000 time steps per flapping cycle is selected for further computations. The same mesh and time step is employed for the cases at Re = 12 and 400. This combination gives a maximum CFL of less than 0.5 for all the simulations. Validation is also performed against the experimental and CFD results of Vandenheede et al. [9], and the results are compared in figure 4 (a) and 4 (b).

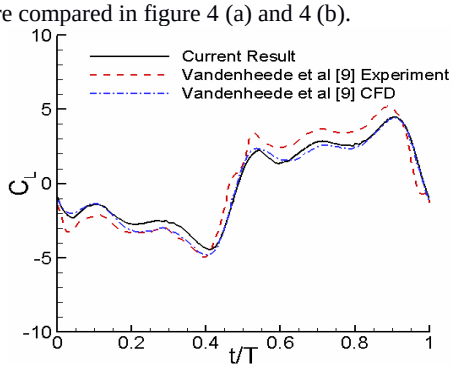

Figure 4 (a). Time history of lift coefficient.

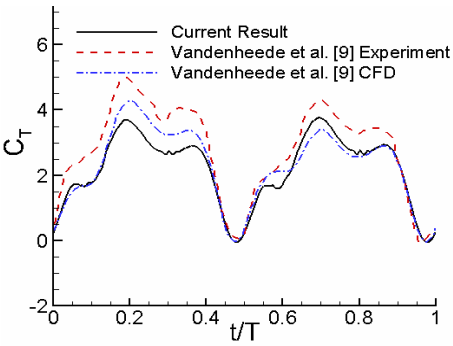

Figure 4 (b). Time history of thrust coefficient.

The time histories of force coefficients show a reasonable agreement with both the experimental and CFD literature results, noting that higher values seen in the experiments are attributed to blockage effects caused by proximity of walls of the apparatus to the wing as mentioned by Vandenheede et al.[9]. The agreement of the C_L history is closer than for C_T, but the timings of the peaks match well in both cases.

Results and Discussions

Comparison of Force Coefficients and Power Economy

Figure 5 shows a comparison of C_L time histories for the four different wing shapes in figure 1. All the wings follow a similar trend of force history at a given Re. For a particular wing shape, the peak value of C_L increases with increasing Re. Similarly, wings with larger area outboard (higher $\bar{r_1}$) record a higher peak C_L. Among all the cases, the highest value of peak C_L (2.191) is achieved by the $\bar{r_1}$ = 0.63 wing at Re = 13500. During supination and pronation (just prior to t/T = 0.5 and 1.0 respectively), the value of C_L drops to a minimum. At Re = 12, the $\bar{r_1}$ = 0.63 wing records the lowest value of C_L (-0.211). While the difference of C_L is obvious at Re = 12, all the wings produce comparatively similar values of C_L at Re = 400 and Re = 13500 at the stroke reversal.

At Re = 12, the increase in C_L is flatter during the down and up strokes, and the lift curves of the rectangular and $\bar{r_1}$ = 0.53 wings are strikingly similar. This may be due to the similarity in the values of the $\bar{r_1}$ of both wings. Hence, the value of $\bar{r_1}$ may be important in determining performance of a wing. At Re = 400

and 13500, the C_L curves are steeper during the down and up strokes, resulting in higher values of peak C_L.

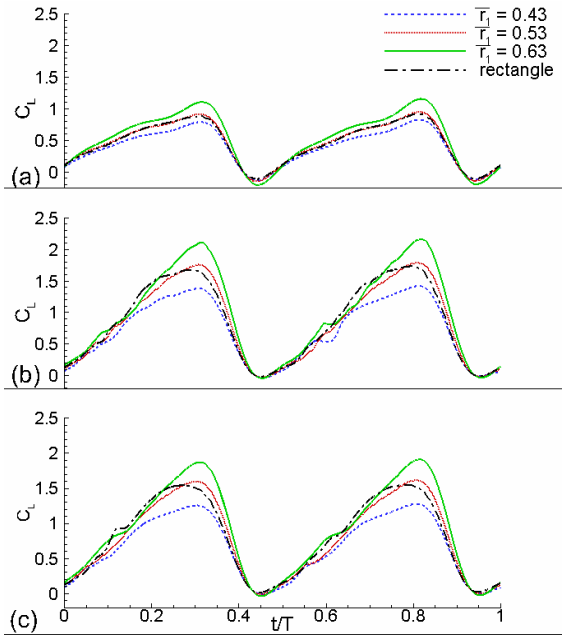

Figure 5. Time history of C_L of all wings at (a) Re = 12 (b) Re = 400 and (c) Re = 13500.

The time histories of the rectangular and $\bar{r}_1$ = 0.53 wings are very close at all Reynolds numbers, but particularly so at Re = 12. The comparison of $\overline{C_L}$ and $\overline{C_P}$ of all wings averaged over the 4th, 5th, and 6th flapping cycles is given in table 2.

Re	Planform	$\overline{C_L}$	$\overline{C_P}$	$\overline{C_L}/\overline{C_P}$
12	$\bar{r}_1$ = 0.43	0.395	1.071	0.369
	$\bar{r}_1$ = 0.53	0.464	1.310	0.354
	$\bar{r}_1$ = 0.63	0.539	1.632	0.330
	Rectangle	0.459	1.290	0.356
400	$\bar{r}_1$ = 0.43	0.664	0.748	0.888
	$\bar{r}_1$ = 0.53	0.801	0.991	0.808
	$\bar{r}_1$ = 0.63	0.913	1.274	0.717
	Rectangle	0.810	0.957	0.846
13500	$\bar{r}_1$ = 0.43	0.719	0.761	0.945
	$\bar{r}_1$ = 0.53	0.871	1.020	0.854
	$\bar{r}_1$ = 0.63	0.996	1.317	0.756
	Rectangle	0.874	0.983	0.889

Table 2. Comparison of lift force, power and power economy of all the wings at Re = 12, 400 and 13500.

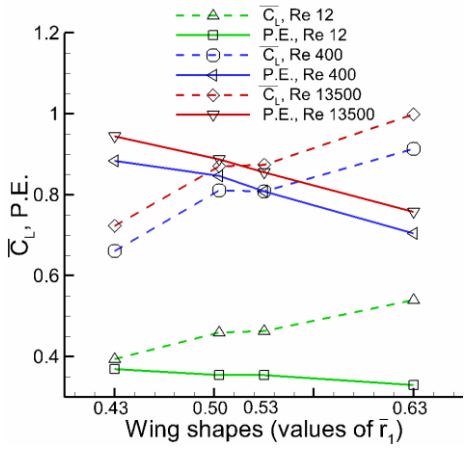

Figure 6. Variation of $\overline{C_L}$ and power economy (P.E.) of different wings at Re = 12, 400 and 13500. $\bar{r}_1$ = 0.50 represents the rectangular wing.

Power economy (P.E.) defined in equation 7 has been used to measure the efficiency of lift production of the wings.

$$P.E. = \overline{C_L}/\overline{C_P} \tag{7}$$

Here $\overline{C_L}$ is the mean coefficient of lift and $\overline{C_P}$ is the mean coefficient of aerodynamic power. At Re = 12, the P.E. of the rectangle and $\bar{r}_1$ = 0.53 wings are the same, which is consistent with the time histories presented in figure 5. At all Re values considered, $\overline{C_L}$ and $\overline{C_P}$ increase with increasing outboard wing area, but the P.E. decreases as shown in figure 6. This result is consistent with the findings of Ansari et al. [1] and the computational study of Wilkins [10] at Re =500. While Ansari et al. [1] did not take into account the wing tip effects, some aspects of viscosity and the effects of spanwise flow, this study confirms that their results still hold valid after considering those factors in the simulations. Thus, wings with lower area outboard are more efficient, irrespective of the Re. However, any given wing must still produce enough lift to keep the insect aloft. In order to elaborate this point, figure 7 shows the variation of P.E. with $\overline{C_L}$ as a function of Re, for all the wings. For example, if a $\overline{C_L}$ of 0.8 is required to balance the weight in hovering motion at Re = 400, then a rectangular wing would serve the purpose. Although it is more efficient in general, the $\bar{r}_1$ = 0.43 wing is unable to produce enough lift for this condition. Hence Re must be considered in conjunction with the wing area distribution to achieve hovering flight. Reasons for this are explored further below.

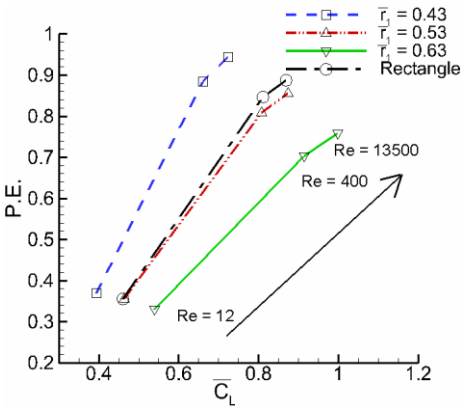

Figure 7. P.E. Vs $\overline{C_L}$ for different wings and Re.

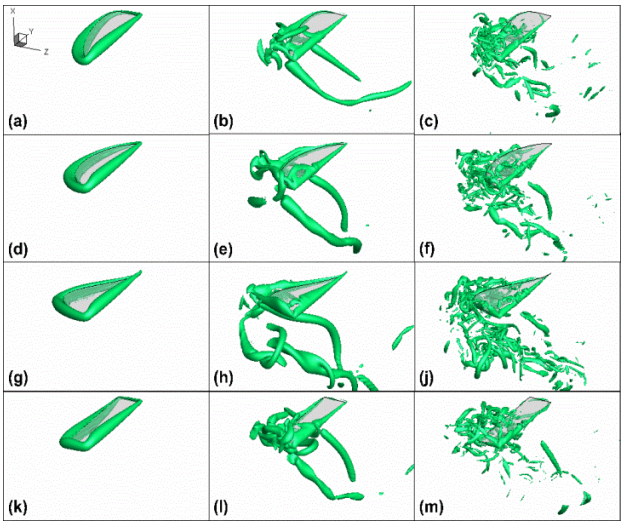

Figure 8. Comparison of iso-Q surfaces at t/T = 0.1. Re = 12 (left), 400 (centre) and 13500 (right). $\bar{r}_1$ = 0.43 wing (a-c), $\bar{r}_1$ = 0.53 wing (d-f), $\bar{r}_1$ = 0.63 wing (g-j) and rectangular wing (k-m).

Comparison of Flow Features

The vortex structures on the wings are visualized in the 6th flapping cycle, (at t/T = 0.1 and 0.3) using Q-criterion iso-surfaces. Non dimensional Q values of 0.5, 5 and 20 are used for Re = 12, 400 and 13500 respectively.

In figure 8, at t/T = 0.1, the wing is about to complete pronation and start the downstroke. At Re = 12, there is a stable, coherent and attached root vortex (RV), leading edge vortex (LEV), trailing edge vortex (TEV) and tip vortex (TV) system, forming a horseshoe shaped structure wrapped around the wings. At Re = 400, a conical LEV structure is developing, as the wing moves through the wake of the previous stroke. At Re = 13500, small-scale vortical structures are observed on the tip and trailing edge and the wake from the previous stroke is relatively intense. The LEV is only just developing for each of the wings, with the RV only visible on the $\bar{r}_1$ = 0.63 wing.

In figure 9, at t/T = 0.3, the wing is in downstroke phase of flapping. At Re = 12, all the wings continue to exhibit a smooth RV, LEV, TEV and TV system, which has grown in size, and there are no signs of vortex shedding. At Re = 400, a stable LEV is anchored on the wing, and it joins the TV in the wake forming a tube like structure. While the RV detaches quickly from the r_1 = 0.53 and r_1 = 0.63 wings, it extends downstream in the wake and joins the LEV-TV trail for the $\bar{r}_1$ = 0.43 and rectangular wings. The LEV on the $\bar{r}_1$ = 0.43 wing shows early signs of vortex breakdown, however, on the other wings it remains attached and sheds close to the wing tip. At Re =13500, a RV is observed on all the wings for the first time. One LEV originates from the wing root, and it splits into a dual LEV system. The formation of dual LEVs at a high Re is consistent with findings in the literature [4]. The front LEV extends along the span and joins the trailing edge, whereas the rear LEV breaks down at about mid span. LEV, TEV and TV shed into a wake, forming a strong helical structure. Although the RV detaches quickly from the $\bar{r}_1$ = 0.53 and $\bar{r}_1$ = 0.63 wings, it joins the LEV, TEV and TV trail in the case of the $\bar{r}_1$ = 0.43 and rectangular wings.

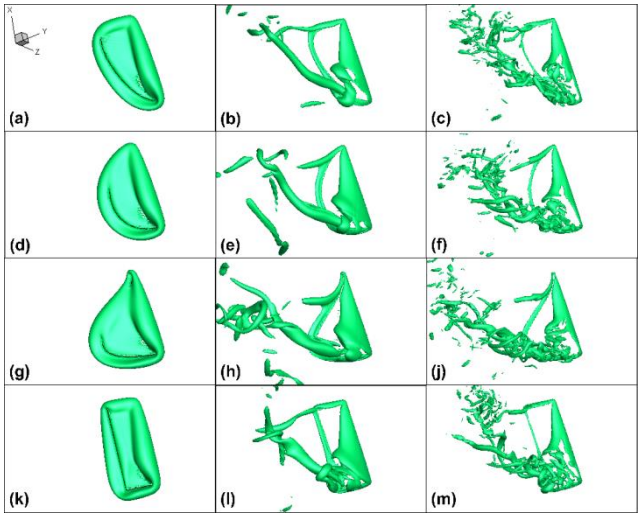

Figure 9. Comparison of iso-Q surfaces at t/T = 0.3. Re = 12 (left), 400 (centre) and 13500 (right). $\bar{r}_1$ = 0.43 wing (a-c), $\bar{r}_1$ = 0.53 wing (d-f), $\bar{r}_1$ = 0.63 wing (g-j) and rectangular wing (k-m).

Conclusion

In this paper, comparison of lift (average, peak and time history), power economy and vortex structures for four equal area wings at three Reynolds numbers has been presented. It was found that average and peak lift coefficients increased with increasing distribution of the wing area outboard, as was expected given the greater wing velocity towards the tip. This also resulted in greater power requirements leading to reduction of power economy. The time history of C_L and P.E. of the rectangular wing was similar to the $\bar{r}_1$= 0.53 wing especially at Re = 12. Both the wings have similar values of $\bar{r}_1$. Hence, $\bar{r}_1$ may be important in determining the performance of a wing especially at low Re. However, further work has to be done to authenticate this result. For a given wing shape, as Re was increased, the vortical structures transformed from a horse-shoe shaped vortex system (Re = 12) to a conical LEV with tube like TV-TEV system (Re = 400), and then to a dual LEV system with helical TV-TEV structures (Re = 13500). Despite the differences in the evolution of flow features at different Re, the performance trend of the various wing shapes was the same that is for a given wing area, wing with less of that area outboard was more efficient.

At a given Re, there was similarity in global flow structure on all the wings [6, 7] which was also confirmed by the resemblance in the pattern of the lift time histories. However, this doesn't qualify as the criterion to gauge the performance of wings, rather it is the placement of wing area in relation to those structures that is determinant of lift and power economy.

Acknowledgment

This research was undertaken with the assistance of resources provided at the Australian National Computational Infrastructure National Facility (NCI-NF) through the National Computational Merit Allocation Scheme.

References

[1] Ansari, S.A., Knowles, K. & Zbikowski, R., Insectlike flapping wings in the hover part II: Effect of wing geometry, *Journal of Aircraft*, **45**(6), 2008, 1976-1990.

[2] Canchi, T., *Numerical Simulation of Unsteady Aerodynamics in Insect Flight Using Generic Planform Shapes*, University of New South Wales, Australian Defence Force Academy, School of Engineering & Information Technology, 2012.

[3] Ellington, C., The aerodynamics of insect flight. II. Morphological parameters, *Phil. Trans. R. Soc. Lond. B*, **305**, 1984, 17-40.

[4] Lu, Y., Shen, G.X. & Lai, G.J., Dual leading-edge vortices on flapping wings, *Journal of experimental biology*, **209**(24), 2006, 5005-5016.

[5] Luo, G. & Sun, M., The effects of corrugation and wing planform on the aerodynamic force production of sweeping model insect wings, *Acta Mechanica Sinica*, **21**(6), 2005, 531-541.

[6] Ozen, C. & Rockwell, D., Flow Structure on a Rotating Wing: Effect of Wing Aspect Ratio and Shape, *51st AIAA Aerospace Sciences Meeting including the New Horizons Forum and Aerospace Exposition*, 2013.

[7] Phillips, N., Knowles, K. & Lawson, N., Effect of wing planform shape on the flow structures of an insect-like flapping wing in Hover, *27th International Congress of the Aeronautical Sciences. ICAS*, 2010.

[8] Tian, F.-B., Dai, H., Luo, H., Doyle, J.F. & Rousseau, B., Fluid–structure interaction involving large deformations: 3D simulations and applications to biological systems, *Journal of computational physics*, **258**, 2014, 451-469.

[9] Vandenheede, R.B., Bernal, L.P., Morrison, C.L., Gogulapati, A., Friedmann, P.P., Kang, C.-K. & Shyy, W., Experimental and Computational Study on Flapping Wings with Bio-Inspired Hover Kinematics, *AIAA Journal*, **52**(5), 2014, 1047-1058.

[10] Wilkins, P.C., *Some unsteady aerodynamics relevant to insect-inspired flapping-wing micro air vehicles*, Cranfield University, 2008.